Journal of Physics: Conference Series **518** (2014) 012025 doi:10.1088/1742-6596/518/1/012025

Formation mechanism of metal embedded amorphous silicate nanoparticles by induction thermal plasmas

M Tanaka[1], J Noda[1], T Watanabe[2], J Matsuno[3], and A Tsuchiyama[3]

[1] Dept. Environmental Chemistry and Engineering, Tokyo Institute of Technology, Yokohama, Japan
[2] Dept. Chemical Engineering, Kyushu University, Fukuoka, Japan
[3] Dept. Geology and Mineralogy, Kyoto University, Kyoto, Japan

watanabe@chem-eng.kyushu-u.ac.jp

Abstract. The purpose of this paper was to synthesize metal embedded amorphous silicate nanoparticles by induction thermal plasmas. Powder of Fe, Ni, Sn, and Zn were used as precursor as well as SiO_2 and MgO. In the case of Fe, Ni, and Sn, metal embedded nanoparticles were successfully synthesized. While most of Zn nanoparticles were attached on the surface of the amorphous silicate nanoparticles. Internal rate of each metal in the synthesized nanoparticles and nucleation temperature were evaluated to understand the formation mechanism of the metal embedded amorphous silicate nanoparticles. Results indicated that the relationship between the nucleation temperature of silicon and the melting temperature of each metal has important role on the metal embedded nanoparticles formation.

1. Introduction

Induction thermal plasmas has many unique advantages including high enthalpy, high chemical reactivity, large plasma volume, long residence time, and selective oxidation or reduction atmosphere according to the required chemical reactions. The high temperature of thermal plasma enables the evaporation of a large amount of raw materials even with high melting and boiling temperatures [1-3]. The formation of nanoparticles in supersaturated state by homogeneous nucleation and heterogeneous condensation can be accomplished due to the rapid quenching rate in the tail flame [4-7]. Furthermore, it is available to synthesize nanoparticles with high purity by RF thermal plasma, because the thermal plasma is generated in the torch without an internal electrode. In the present work, synthesis of metal embedded amorphous silicate nanoparticles by RF thermal plasmas was tried based on following motivations.

First, crystalline silicate in circumstellar regions and in primitive materials of the solar system is believed to be crystallized from amorphous silicates. GEMS (glass with embedded metal and sulfide) is a major component of cometary dust. According to recent work [8], GEMS is composed of amorphous silicate including iron metal in the size of few tens of nanometer. The alteration experiments with GEMS analogue materials are required to understand the evolution of amorphous silicate in the early solar system.

Second, the metal nanoparticles are expected to be applied in magnetic storage media, nanosensors and devices, drug delivery system and so on. However, the metal nanoparticles are difficult and dangerous to handle due to their instability and high reactivity. Therefore, surface coated metal

nanoparticles have attracted to solve this issue. In particular, amorphous silicate as shell material could be useful because of its high thermal resistance and corrosive properties.

The objective of the present work is to synthesize the metal embedded amorphous silicate nanoparticles by induction thermal plasma. Another purpose is to investigate the formation mechanism of metal embedded amorphous silicate nanoparticles. The different metals are tried to synthesize the objective nanoparticles.

2. Experimental procedure

2.1. Experimental setup

Figure 1 shows experimental setup for metal embedded amorphous nanoparticles preparation, which is composed of the RF torch and the synthesis chamber. Precursors of metal, SiO_2, and MgO powders with particle size of several micrometers are injected from the powder feeder by Ar carrier gas. Different metals including Fe, Sn, Ni, and Zn were compared to investigate the formation mechanism. The composition ratio of metal to Si was 0.56, which was adjusted based on the GEMS mean composition. The powder feed rate was fixed at 250 mg/min. The input power of RF thermal plasma was controlled around 30 kW. Argon was used for the carrier gas of the raw powder, and argon and helium were used for plasma forming gases to evaporate the raw materials efficiently. Table 1 shows operating conditions for the synthesis system. In these experimental conditions, complete evaporation of the raw materials was confirmed by SEM observation.

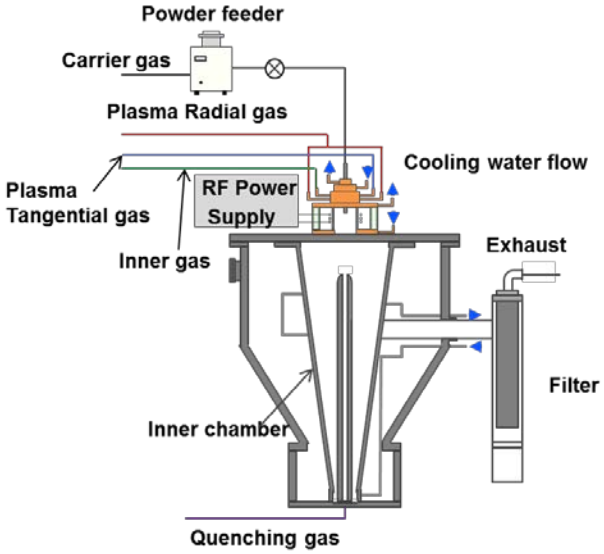

Figure 1. Experimental setup for the synthesis of metal embedded nanoparticles

2.2. Analyses

The phase identification of the prepared nanoparticles were determined by X-ray diffractometry (XRD, Miniflex, Rigaku Co.) operated with Cu Kα source (λ = 0.1541 nm). The diffraction data was collected using a continuous scan mode with speed of 4 degree/min in the region 10–90degree with a step size of 0.04degree. The accelerating voltage and applied current was 40 kV and 50 mA, respectively.

The particle morphology and size distribution of synthesized nanoparticles were observed using a TEM (S4700, Hitachi Ltd.) operating at an accelerating voltage of 5 kV.

Surface composition was measured by X-ray photoelectron spectroscopy (XPS, 1700R ESCA system, ULVAC-PHI Inc.), while inductively coupled plasma atomic emission spectroscopy (ICP-AES, ICPS-8100, Shimadzu Co.) was used to measure the composition of each element in the synthesized nanoparticles.

Table 1 Operating conditions for synthesis of metal embedded nanoparticles

Plasma power plate	30 kW
Frequency	4 MHz
Pressure	101.3 kPa
Sheath gas 1	Ar 60 L/min
Sheath gas 2	He 5 L/min
Inner gas	Ar 5 L/min
Carrier gas	Ar 6.5 L/min
Raw Material	Me, MgO, SiO_2
Me/Si	0.56
Me	Fe, Ni, Sn, or Zn
Feeding rate	250 mg/min

3. Results and discussion

XRD spectra of synthesized nanoparticles in different systems are presented in Figure 2. The diffraction peaks of Si, Mg, and their oxides were not observed. In contrast, the diffraction peaks of each metal, Fe, Sn, Ni, and Zn, were found in different systems. These results indicate that SiO_2-MgO silicate and metal co-exist in the synthesized nanoparticles. In the cases of Ni and Zn, the diffraction peaks of metal oxide were also observed. This will be discussed in following section.

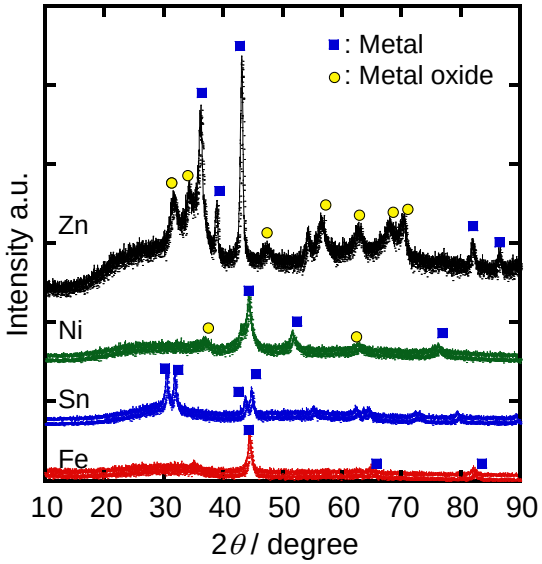

Figure 2. XRD spectra of the synthesized nanoparticles from different metal precursors.

TEM images of the synthesized nanoparticles in Fe-SiO_2-MgO system are presented in Figure 3. Core/shell structured nanoparticles were observed as shown in Figure 3 (a). Additional energy dispersive spectrometer (EDS) analysis revealed that the core contains Fe, while the shell part are composed of Si, Mg, and O. Figure 4 represents TEM images of the synthesized nanoparticles in different systems. In the case of Sn and Ni, core/shell structured nanoparticles were also observed as well as Fe case. While, Zn nanoparticles were not found in core of synthesized nanoparticles. The particle mean diameters of the main amorphous silicates were in the range from 29 nm to 34 nm in different metal-SiO_2-MgO systems. The effect of additional metals on the diameter of the amorphous silicate nanoparticles was not confirmed.

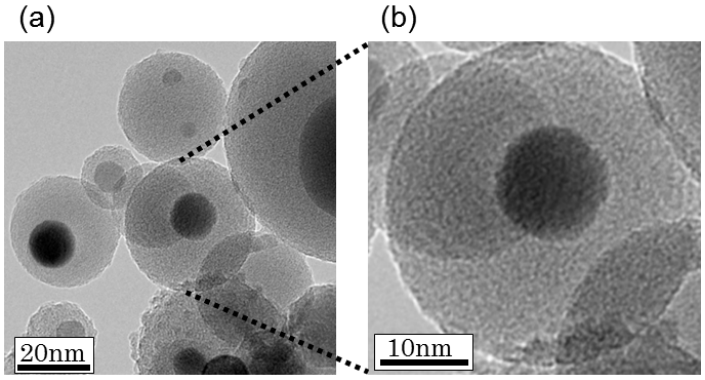

Figure 3. TEM images of Fe embedded nanoparticles synthesized by RF thermal plasmas.

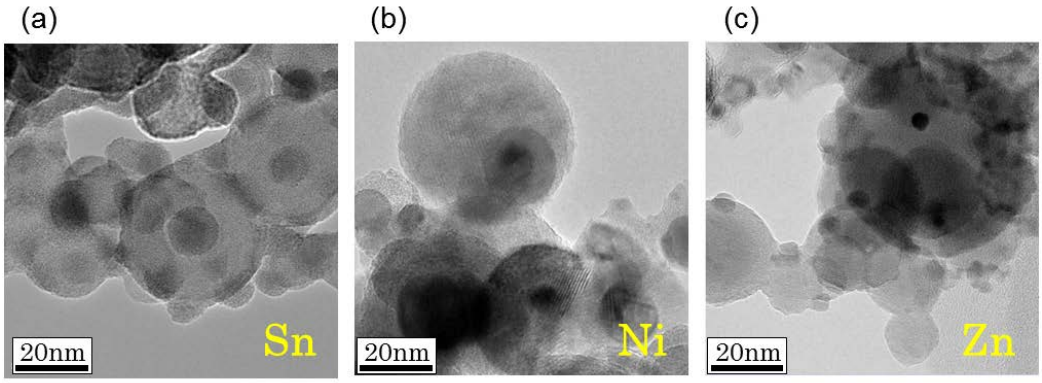

Figure 4. TEM images of synthesized nanoparticles from different precursors: (a) Sn-SiO_2-MgO, (b) Ni-SiO_2-MgO, (c) Zn-SiO_2-MgO.

Figure 5 shows the mole fraction of each metal in the synthesized nanoparticles measured by ICP-AES and that in the surface region of the synthesized nanoparticles measured by XPS. Since the mole fractions in the synthesized nanoparticles in different systems were determined by the initial composition of the raw material, these values were almost same among the used metals. In contrast, the mole fractions of each metal in the surface region of the synthesized nanoparticles were varied in different systems. The mole fraction of Fe in the surface region was lowest than other metals. This result suggests that the Fe nanoparticles were successfully coated by the shell of the amorphous silicate. In the case of Zn, the mole fraction of Zn in the surface region of the nanoparticles was higher than that in the whole nanoparticles. This result indicates that Zn nanoparticles were not coated by the amorphous silicate. This result also can be used to explain the reason of the existence of zinc oxide, as presented in the XRD spectrum. Zn nanoparticles were oxidized by the surrounding air because Zn nanoparticles were not coated by the amorphous silicate.

Internal rate of each metal was defined to evaluate the amount of the fully coated metal quantitatively. Internal rate is the ratio of coated metal to total metal in the synthesized nanoparticles. It was calculated based on the volume ratio between the metals in the surface of the particles and that in the whole particles. Figure 6 shows the internal rate of each metal in different systems. Internal rate of Fe was highest, while that of Zn was lowest. This trend has good agreement with the results of other analyses mentioned above. To discuss the reason of different internal rates among used metals in the present work and the formation mechanism of the metal embedded amorphous silicate nanoparticles, the nucleation temperature was evaluated based on the homogeneous nucleation model.

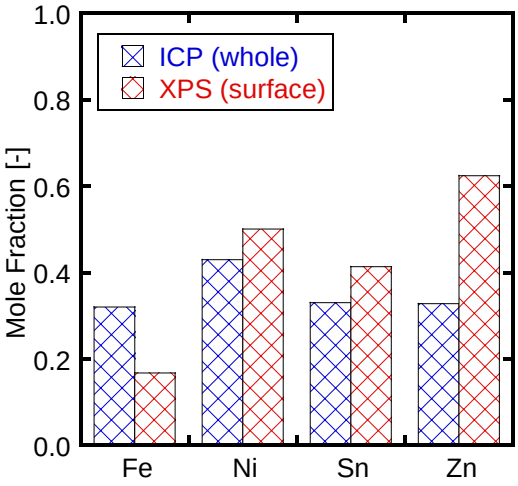

Figure 5. Mole fraction of each metal in surface region and whole region of the synthesized nanoparticles.

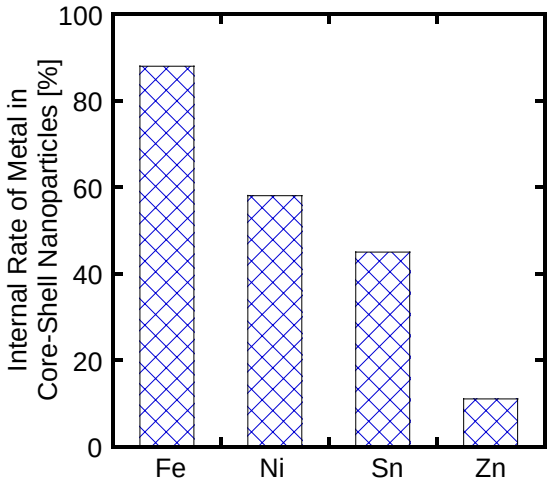

Figure 6. Internal rate of each metal in the synthesized nanoparticles from different precursors.

Girshick et al. derived the homogeneous nucleation models as an extension of the kinetic nucleation theory [9]. The proposed model which is shown in Equation (1) was used for the estimation of the critical saturation ratio.

$$J = \frac{\beta_{ij} n_s^2 S}{12} \sqrt{\frac{\Theta}{2\pi}} \exp\left(\Theta - \frac{4\Theta^3}{27(\ln S)^2}\right) \tag{1}$$

where n_s is the equilibrium saturation monomer concentration at temperature T, β is the collision frequency function between monomers, and S is the saturation ratio. The dimensionless surface tension Θ is given by the following Equation:

$$\Theta = \frac{\sigma s_1}{kT} \tag{2}$$

where σ is the surface tension and s_1 is the monomer surface area. The collision frequency function can be estimated using Equation (3) as follows:

$$\beta_{ij} = \left(\frac{3v_1}{4\pi}\right)^{1/6} \sqrt{\frac{6kT}{\rho_P}\left(\frac{1}{i}+\frac{1}{j}\right)} \times \left(i^{1/3} + j^{1/3}\right)^2 \tag{3}$$

where ρ_p is the particle mass density and v_1 is the monomer volume. Since the particle is nucleated by the monomer collision in this model, i and j are equal to 1. The nucleation rate is strongly dependent on the surface tension and the saturation ratio. Particle formation is observed experimentally when the nucleation rate is over 1.0 $cm^{-3}s^{-1}$. Hence, the corresponding value of the saturation ratio is defined as the critical saturation ratio.

The nucleation temperature at the critical saturation ratio is presented in Figure 7 as well as melting and boiling points. Because of the unknown properties of the silicon oxide, only melting and boiling points of SiO and SiO_2 are plotted without nucleation temperature. As shown in Figure 7, nucleation temperature of Si was highest among that of the considered species. Furthermore, the melting point of SiO and SiO_2 were higher than the nucleation temperature of considered other metals of Fe, Ni, Sn, and Zn. These results indicate that the silicon or its oxide firstly nucleated and other species except Zn then co-condensed on the nuclei. Finally, the metals are considered to start solidification in the molten silicate in the quenching process to form the metal embedded amorphous silicate nanoparticles. Zn has the lowest boiling point, which is lower than the melting point of silicate. Therefore, Zn vapour cannot condense on the silicate particles. These results can explain the obtained experimental results.

However, the difference among Fe, Ni, and Sn has not been understood yet and is under investigation. In this study, the relationship between the nucleation temperature and melting and boiling point was considered to discuss the formation mechanism. In the future study, the effect of the temperature decay rate, temperature history, on the formation mechanism will be investigated.

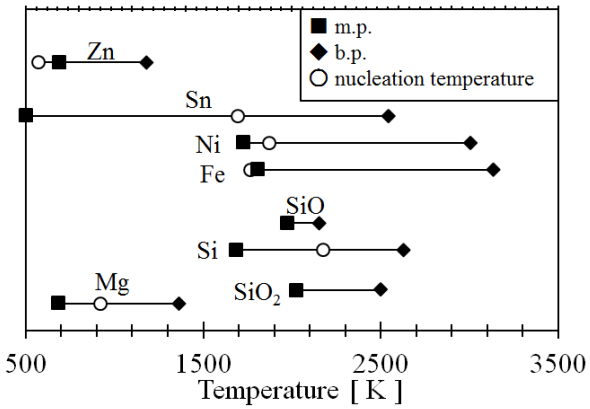

Figure 7. Nucleation temperature, melting and boiling points of considered species.

4. Conclusion

The metal embedded amorphous silicate nanoparticles as an analogue material of GEMS were successfully synthesized in RF thermal plasma process. Internal rate and nucleation temperature of each metal were evaluated to discuss the formation mechanism of the metal embedded nanoparticles. In the case of Fe, the highest internal rate of 90% was obtained, while the internal rate of Zn was less than 20%. This difference can be explained by the relationship between the nucleation temperature of metal and that of silicon or silicon oxide. The synthesized metal embedded nanoparticles as an analogue materials of GEMS would help to reveal the evolution of amorphous silicate in the early solar system. Furthermore, synthesized nanoparticles as surface coated metal nanoparticles would be applied in nanomagnetic field.

References

[1] Watanabe T, Nezu A, Abe Y, Ishii Y and Adachi K 2003 *Thin Solid Films* **435** 27
[2] Watanabe T and Okumiya H 2004 *Sci. Technol. Adv. Mater.* **5** 639
[3] Szepvolgyi J, Markovic Z, Scheier P and Feil S 2006 *Plasma Chem. Plasma Process.* **26** 597
[4] Shigeta M and Watanabe T 2005 *J. Mater. Res.***20** 2801
[5] Desilets M, Bilodeau JF and Proulx P 1997 *J. Phys. D: Appl. Phys.* **30** 1951
[6] Gonzalez NYM, Morsli ME and Proulx P 2008 *J. Therm. Spray Technol.* **17** 533
[7] Shigeta M and Watanabe T 2010 *J. Appl. Phys.* **108** 043306
[8] Kemper F, Vriend WJ and Tielens AGGM 2004 *Astrophys. J.* **609** 826
[9] Girshick SL, Chiu CO and McMurry PH 1990 *Aerosol Sci. Technol.* **13** 465